



Extratropical Cyclone Clouds in the GFDL Climate Model: Diagnosing Biases and the Associated Causes

CATHERINE M. NAUD

Department of Applied Physics and Applied Mathematics, Columbia University/NASA Goddard Institute for Space Studies, New York, New York

JAMES F. BOOTH AND JEYAVINOTH JEYARATNAM

Department of Earth and Atmospheric Sciences, City College of New York, City University of New York, New York, New York

LEO J. DONNER, CHARLES J. SEMAN, AND MING ZHAO

NOAA/Geophysical Fluid Dynamics Laboratory, Princeton, New Jersey

HUAN GUO

University Corporation for Atmospheric Research/Cooperative Programs for the Advancement of Earth System Science, NOAA/Geophysical Fluid Dynamics Laboratory, Princeton, New Jersey

YI MING

NOAA/Geophysical Fluid Dynamics Laboratory, Princeton, New Jersey

(Manuscript received 6 June 2019, in final form 16 July 2019)

ABSTRACT

The clouds in Southern Hemisphere extratropical cyclones generated by the GFDL climate model are analyzed against MODIS, *CloudSat*, and *CALIPSO* cloud and precipitation observations. Two model versions are used: one is a developmental version of “AM4,” a model GFDL that will utilize for CMIP6, and the other is the same model with a different parameterization of moist convection. Both model versions predict a realistic top-of-atmosphere cloud cover in the southern oceans, within 5% of the observations. However, an examination of cloud cover transects in extratropical cyclones reveals a tendency in the models to overestimate high-level clouds (by differing amounts) and underestimate cloud cover at low levels (again by differing amounts), especially in the post-cold frontal (PCF) region, when compared with observations. In focusing only on the models, it is seen that their differences in high and midlevel clouds are consistent with their differences in convective activity and relative humidity (RH), but the same is not true for the PCF region. In this region, RH is higher in the model with less cloud fraction. These seemingly contradictory cloud and RH differences can be explained by differences in the cloud-parameterization tuning parameters that ensure radiative balance. In the PCF region, the model cloud differences are smaller than either of the model biases with respect to observations, suggesting that other physics changes are needed to address the bias. The process-oriented analysis used to assess these model differences will soon be automated and shared.

1. Introduction

Over the past decade, cloud cover biases in the Southern Hemisphere oceans have been identified (Trenberth

and Fasullo 2010) and investigated in a large number of general circulation models (GCMs) and reanalysis products. Bodas-Salcedo et al. (2012, 2014) demonstrated that biases in shortwave absorption at the surface (an issue dominating during the austral summer) stem from deficiencies in the low and midlevel clouds typically found in the cold sector of extratropical cyclones. Coincidentally

Corresponding author: Catherine M. Naud, cn2140@columbia.edu

DOI: 10.1175/JCLI-D-19-0421.1

© 2019 American Meteorological Society. For information regarding reuse of this content and general copyright information, consult the [AMS Copyright Policy \(www.ametsoc.org/PUBSReuseLicenses\)](https://www.ametsoc.org/PUBSReuseLicenses).

Naud et al. (2014) showed that recent versions of reanalyses do not have enough clouds in extratropical cyclone cold sectors. This underestimate in cloud cover over southern oceans was diagnosed in models from both phase 3 and phase 5 of the Coupled Model Intercomparison Project (CMIP3 and CMIP5) and until recently was found to affect most current models (Bodas-Salcedo et al. 2014). That GCMs do not produce enough cloud in the southern oceans is problematic: it causes errors in the amount of shortwave radiation reaching the ocean surface (Trenberth and Fasullo 2010) and biases in atmospheric circulation change predictions (e.g., Ceppi and Hartmann 2016; Grise and Medeiros 2016) and ultimately affects climate sensitivity in models (Frey and Kay 2018). Most specifically for ocean–atmosphere coupled models, the cloud bias can affect southern ocean ventilation and the location of the intertropical convergence zone (e.g., Xiang et al. 2018).

One potential reason behind this persistent problem was attributed to the ubiquitous presence of supercooled water in Southern Hemisphere (SH) clouds (Morrison et al. 2011) which models have problems maintaining (Kay et al. 2016). By forcing their model to maintain liquid in clouds for temperatures below freezing, Kay et al. (2016) could correct the surface absorption issue. However, while an advanced treatment of boundary layer clouds in another model improved Southern Hemisphere cloud liquid amounts, its cloud cover bias persisted (Wall et al. 2017; Song et al. 2018).

These recent studies focused on both the microphysical and macrophysical aspects of cloud representation but there might be other aspects of model cloud parameterization that need to be investigated before the SH cloud cover bias can be understood and corrected, such as the representation of boundary layer processes and convection. Here we focus on convection. This is motivated in part by recent work of Lamraoui et al. (2019), who find that, at the typical spatial resolution of a GCM, cloud cover in cyclone cold sectors is responding more strongly to changes in the convection than the boundary layer parameterizations. However, these results were obtained with the Weather Research Forecasting model for a single case study, so it is uncertain whether the impact of convection parameterization is as large in a global-scale multiyear GCM integration.

Another related issue discussed in the Kay et al. (2016) and Frey and Kay (2018) studies resides with the impact of the various parameters that need to be set in the models to keep them in radiative balance. While these parameters are chosen to be as realistic as possible, their exact values are not always precisely known or constant in nature (Hourdin et al. 2017; Schmidt et al. 2017), and small changes in these tuning parameters can have large impacts on cloud cover and other fields important for accurate future temperature predictions

(e.g., Golaz et al. 2013; Zhao et al. 2018b), in part because of the nonlinear nature of the model physics.

Because these two issues cannot easily be untangled, the goal of this study is therefore to examine both the impact of the convection parameterization and of the tuning of cloud parameters on the model representation of cloud cover in the cold sector of extratropical cyclones. To do this, we take advantage of metrics designed to evaluate modeled cloud cover in the cold sector of extratropical cyclones (e.g., Naud et al. 2014, 2015, 2016) and apply them to two separate development versions of the Geophysical Fluid Dynamics Laboratory (GFDL) Atmosphere model, version 4 (AM4). These two versions were produced at different stages of the latest GFDL AM4 model development (Zhao et al. 2018a,b), one of the major U.S. climate models slated to be part of the next CMIP exercise (phase 6). The main differences that matter for the clouds between the two model versions are the parameterization of convection and the tuning applied in the cloud parameterization that ensures radiative balance. The convective parameterizations are a two-plume model as used in the most recent release of the model AM4.0 described in Zhao et al. (2018a,b) and a multiplume model as described in Donner et al. (2011).

Herein, we compare both versions of the model to cloud cover observations obtained with the Moderate Resolution Imaging Spectroradiometer (MODIS; Salomonson et al. 1989) and the two active instruments on board *CloudSat* (Stephens et al. 2002) and *CALIPSO* (Winker et al. 2009). The method is based on compositing, using the center of extratropical cyclones as anchors to obtain the mean cloud cover for a large number of systems, which was shown to be a useful method for comparison with free-running models (e.g., Klein and Jakob 1999; Bauer and Del Genio 2006; Field et al. 2008, 2011; Govekar et al. 2014). We also introduce cold-front-centered vertical transects, which have also been used for model evaluation (Naud et al. 2010; Booth et al. 2013). These composite transects were found particularly useful when using *CloudSat* and *CALIPSO* observations, which provide full cloud profiles but, with their narrow footprint, only partly sample frontal regions. The focus is on the cold-frontal regions of extratropical cyclones located in the southern oceans during the warm season (when insolation is at a maximum).

2. Model, observations, and method

For model and observations, the analysis is performed only from November to March and solely for the Southern Hemisphere oceans.

a. Model description

The versions of the GFDL model examined here are intermediate development versions of the GFDL model that

precedes AM4.0 (Zhao et al. 2018a,b) and are generically referred to as devAM4. The focus is the parameterization of convection, and both devAM4 and AM4.0 represent convection using the same modified mass flux scheme originally developed for shallow convection (Bretherton et al. 2004). The original Bretherton et al. (2004) scheme utilizes a single bulk plume that entrains and detrains at each model layer. While the lateral mixing rate is largely specified, the vertical profile of entrainment/detrainment rate is determined interactively by a parcel buoyancy sorting algorithm so that the cloud vertical mass flux can either increase or decrease with height depending on the thermodynamic properties of cloud environment.

Attempts at using the single bulk plume model for representing both shallow and deep convection met with some success at a high (50 km) resolution (Zhao et al. 2009). However, during the development of AM4/CM4, it was found that some aspects of coupled model biases (e.g., equatorial Pacific cold bias) could be significantly reduced by including an additional deep plume with a reduced lateral mixing rate. The motivation of including such an additional deep plume is discussed in Zhao et al. (2016) and Zhao et al. (2018b). Below we refer to this two-plume scheme as devAM4–2PM, or simply 2PM.

We obtained output from a predecessor version of the devAM4 model that uses, among other differences, a distinct scheme for the parameterization of convection than in devAM4–2PM. This second model version still uses the Bretherton et al. (2004) parameterization for shallow convection, but handles deep convection with a scheme introduced by Donner et al. (2001), which is a multiplume model (Donner et al. 2011). Therefore, this second version of the model will be referred to as the multiplume model devAM4-MPM, or simply MPM.

The devAM4 has the same overall physics parameterizations as AM4.0; however, there are a number of differences in the configuration of the parameterizations. More specifically, we list here the components that differ from what is described in Zhao et al. (2018b): 1) The treatment of convective precipitation and cumulus mixing in devAM4 is similar to that described in Zhao et al. (2016). The total condensate is removed as precipitation, which is then partitioned into liquid and ice phase based on temperature. In addition, the parameterization of lateral mixing rate of the shallow plume was simplified by removing its height dependence. 2) The devAM4 uses a four-stream treatment of shortwave (SW) radiation with a SW radiation time step of 2 h. This choice was not adopted in AM4.0 because of its significant computational cost with little improvement in simulations of radiation fields. 3) The decorrelation length scale in the cloud overlap assumption is set to

1 km in devAM4. 4) The size distribution of sulfate aerosol for computing cloud drop activation in devAM4 follows that described in Donner et al. (2011). 5) The devAM4 has 32 vertical layers instead of the 33 layers used in AM4.0. 6) Convection in stratocumulus clouds can be overactive in the model, so, for AM4.0, convection is turned off whenever the Wood and Bretherton (2006) “estimated inversion strength” (EIS) parameter exceeds 8 K. This test is not implemented in devAM4.

Changing the convection scheme changes the thermodynamics and dynamics in the model, which impacts the clouds and radiation. As such, if we performed integrations using devAM4 with only the convection scheme changed, the model would be significantly inconsistent with the present-day Earth energy imbalance of around 0.7 W m^{-2} (Schmidt et al. 2017). Such a model would not be consistent with all GCMs utilized in IPCC experiments, and the interpretation of the physics would be subject to a strong caveat: a lack of radiative balance. Therefore, some tuning parameters that impact clouds and precipitation had to be changed in MPM, as compared with 2PM, so that MPM is in radiative balance as well. So in the rest of the study, when we mention tuning, we mostly refer to the parameters used in the cloud parameterization (other than moist convection). To help decipher differences between 2PM and MPM that are the consequence of a differing convection scheme rather than cloud tuning parameters, we also introduce two additional model integrations that are out of radiative balance: one devAM4 version with the 2PM convection scheme but tuned with the MPM tuning parameters, hereinafter referred to as 2PM (MPM Tune), and devAM4 with the MPM convection scheme but tuned with 2PM tuning parameters, referred to as MPM (2PM Tune). These supplemental integrations can be considered as an attempt at keeping as much of the MPM/2PM model characteristics but for the convection scheme. In other words, MPM (2PM Tune) includes as many of the 2PM model characteristics as possible but uses the MPM convection scheme (and inversely). The four model integrations examined here are summarized in Table 1.

The primary cloud-parameterization tuning differences between MPM and 2PM that are relevant to our comparison are (see details in Table 2) as follows. 1) There is a larger volume-mean drop radius for auto-conversion of cloud liquid to rain in MPM (10 vs $8 \mu\text{m}$). 2) A larger lower bound on the stratiform subgrid vertical-velocity standard deviation is used for aerosol activation to cloud droplets in MPM (0.7 vs 0.3 m s^{-1}). 3) There is a more rapid erosion of stratiform clouds in 2PM (erosion constants 10 to 140 times larger, depending on whether stratiform clouds co-occur with various combinations of diffusion and convection). 4) The ice

TABLE 1. Summary of the four model integrations, showing naming convention, cumulus scheme, and tuning protocol.

Model denomination	Cumulus scheme	Tuning
2PM	Two-plume model (Zhao et al. 2016, 2018b)	Tuned in general accordance with Zhao et al. (2018b)
MPM	Multiphase model (Donner et al. 2001, 2011)	Tuned in general accordance with GFDL practices described in Schmidt et al. (2017)
2PM (MPM tune)	Two-plume model (Zhao et al. 2016, 2018b)	Tuned in general accordance with GFDL practices described in Schmidt et al. (2017)
MPM (2PM tune)	Multiphase model (Donner et al. 2001, 2011)	Tuned in general accordance with Zhao et al. (2018b)

crystal fall speeds in MPM are two-thirds of those in 2PM. 5) The boundary layer cloud-top radiative cooling generates more entrainment into the boundary layer in MPM than 2PM (buoyancy parameter related to radiation 20% larger). 6) The entrainment in shallow cumulus plumes is 90% larger in MPM than 2PM. 7) Precipitation efficiencies in shallow cumulus plumes are lower in 2PM (e.g., about 25% of the efficiencies in MPM around 800 hPa). As we discuss the differences in clouds for the two models, we will refer back to the changes in tuning parameters to point out when they might be contributing to the changes we find.

Both model versions were run for the same time period (2008–12) and with the same sea surface temperature forcing. The output used here is available at $1.25^\circ \times 1^\circ$ spatial resolution every 6 h and consist of 2D total cloud cover, surface precipitation (total, large-scale, and convective), column integrated precipitable water, 500-hPa vertical velocity, and sea level pressure, as well as vertical profiles on model levels of cloud cover (total, large scale, and convective), geopotential heights, temperature tendencies for convection, relative humidity, temperature, and wind.

GFDL has implemented the Cloud Feedback Model Intercomparison Project (CFMIP) Observation Simulator Package (COSP; Bodas-Salcedo et al. 2011) in its latest operational AM4.0 model (Zhao et al. 2018a). The COSP simulators are developed to take into account known limitations in the observations when comparing with modeled output. However, the simulators were not implemented in the model-development versions examined here. Because our focus here is on differences between two different models, the observations are merely used as a benchmark and are not intended to provide an absolute truth. Therefore, the lack of COSP simulated output is not an impediment for the study and does not qualitatively affect the results and conclusions.

b. Observations

To provide a reference for comparison with model output, cloud observations retrieved with MODIS and *CloudSat/CALIPSO* are used, and meteorological fields (i.e., temperature, wind, precipitable water, and vertical velocities) are obtained from the MERRA-2 reanalysis (Gelaro et al. 2017).

TABLE 2. List of the main tuning parameters that differ between the two devAM4 models, with values. More details on the role of each parameter are available in Zhao et al. (2018b).

Tuning parameter	Expected impact	2PM	MPM
Stratiform cloud erosion constants (s^{-1}): Rates of erosion when vertical diffusion is active	Clouds erode more rapidly when larger	4×10^{-5}	3×10^{-7}
when convection is active without vertical diffusion		4×10^{-5}	3×10^{-6}
when neither convection nor vertical diffusion is active		3×10^{-6}	1×10^{-7}
Volume mean drop radius for autoconversion of cloud liquid to rain (μm)	Clouds precipitate more efficiently when smaller	8	10
Lower bound of the stratiform subgrid vertical velocity standard deviation used for aerosol activation to cloud droplets ($m s^{-1}$)	Cloud drop number concentration tends to increase when larger	0.3	0.7
Ice crystal fall speed ratio	Ice falls out faster when larger	1.2	0.8
Constant in function relating boundary layer cloud-top radiative cooling to boundary layer entrainment	Larger values increase boundary layer entrainment	0.25	0.3
Entrainment in shallow cumulus plumes (km^{-1})	Reduces convective buoyancy when larger	3	5.7
Precipitation efficiency parameters (Pa^{-1}):	Clouds precipitate more efficiently when larger		
Liquid		5×10^{-5}	20×10^{-5}
Ice		11×10^{-5}	44×10^{-5}

In this study, we use both monthly and daily gridded *Aqua* MODIS cloud fraction products (Menzel et al. 2008) from the latest (Collection 6) processing algorithm. This cloud fraction product is initially calculated for 5-km pixels using the 1-km cloud mask (Ackerman et al. 2008) obtained using a series of observed radiances in the visible and infrared channels. The instantaneous 5-km resolution cloud fraction retrievals are then aggregated for the monthly and daily files into a grid of $1^\circ \times 1^\circ$ spatial resolution for all daytime and nighttime orbits and all cloud types. This product's known limitations are misdetections over snow and sea ice, in the sunglint region and at low sun and view angles (Menzel et al. 2008). An evaluation of the MODIS cloud fraction retrievals in extratropical cyclones regions revealed agreements with other similar products within 5% for the southern oceans, but also issues over sea ice and snow covered land that we do not include here (Naud et al. 2013). However, because of the latitudes considered here and the focus on warm months, we expect a minimal impact of these issues on the results. Here we refer to these cloud fractions as total cloud cover to match the model syntax. We collected monthly and daily data for the period overlapping with the model run, 2008–12.

The *CloudSat*/*CALIPSO* cloud profiles are obtained from the GEOPROF-lidar product (Mace and Zhang 2014), which reports up to six cloud layer base and top altitudes in each *CloudSat* footprint ($\sim 1.4 \text{ km} \times 1.7 \text{ km}$; Tanelli et al. 2008). These cloud layer boundaries are obtained by combining *CALIPSO* and *CloudSat* cloud mask products. Here they are used to produce a vertical cloud mask of 250-m vertical resolution along the *CloudSat* orbits. This product is known to experience issues close to the surface because of ground clutter, so the first kilometer above sea level is not examined here. Also, cloud and precipitation cannot be distinguished, so cloud extents can be overestimated (i.e., cloud base might be too low). Here we collected all the data for the period 2006–16, but after 2011 the *CloudSat* radar platform is only operated during daytime. This was found not to affect the analysis (not shown).

Shortwave (SW) and longwave (LW) top-of-atmosphere cloud radiative effect (CRE) are obtained from the NASA Clouds and the Earth's Radiant Energy System (CERES) Energy Balanced and Filled (EBAF) Edition 4.0 product (Loeb et al. 2018).

c. Extratropical cyclones and cold-front identification

Two distinct algorithms are used to 1) identify and track extratropical cyclones and 2) locate cold fronts. The cyclones are identified with the Modeling, Analysis and Prediction (MAP) Climatology of Midlatitude

Storminess (MCMS) algorithm (Bauer et al. 2016) which uses 6-hourly gridded sea level pressure fields to locate storm centers and then track them through the cyclone lifetime. This algorithm has historically been used to create a database of cyclone locations using the ERA-Interim reanalysis (Dee et al. 2011); here we collected locations for the period 2006–16 to match the two cloud datasets described above. The same MCMS algorithm is also applied to the four models (cf. Table 1) sea level pressure fields.

Both 2PM and MPM exhibit a similar total number of 6-hourly cyclone detections. However, MPM tends to detect more cyclone centers north of 40°S while 2PM detects more south of 50°S . These differences in location cause differences in environmental moisture in the vicinity of the cyclones (which in turn can impact cloud cover). This is despite using the same fixed SST forcing in both models. Consequently, when we compare the two model versions, we impose a similar zonal distribution of cyclones in both models. For this, we randomly select cyclone centers in 2° -wide latitude bands to ensure the same total number of cyclones per band in each model.

Cold fronts are identified using an algorithm described in Naud et al. (2016). It is applied to MERRA-2 850-hPa potential temperature gradients using the Hewson (1998) technique to identify cold fronts. For cyclones that have temperature gradients too weak to allow the routine to identify the cold fronts, the method proposed by Simmonds et al. (2012) is applied instead, also using MERRA-2 output. This method locates surface cold fronts based on the change in 850-hPa wind direction and strength as a cold front passes a location. The MERRA-2 reanalysis was chosen because of its relatively high spatial resolution ($0.625^\circ \times 0.5^\circ$) that helps to obtain more precise frontal locations. The MERRA-2-based cold-front identifications are used with cloud observations. The same Naud et al. (2016) algorithm is applied to the four integrations of the devAM4 model (cf. Table 1), making use of the modeled 850-hPa potential temperature and winds.

d. Compositing method

We use composites of cloud cover, as well as other atmospheric variables, over multiple instances of the same type of atmospheric phenomenon to compare the models with observations or reanalysis. We generate two types of composite averages: cyclone centered and cold front centered. The former is a plan view as a passive instrument would observe, while the latter is a vertical transect spanning both sides of the cold front as observed by active instruments. Composites are an average, as such all variability is smoothed out and the

resulting distributions are representing the most salient features and do not necessarily look like any of the individual cases that went into it. However, they present a great advantage for model evaluation as they allow multiple cases to be included and do not necessitate a match in time and space between the free running models and observations.

The cyclone-centered composites are constructed using the same stereographic grid for model output, MERRA-2 products, and MODIS observations, centered on the low pressure minimum of a cyclone, of 100-km radial and 15° angular resolution, and extending out to 2500 km radially (e.g., Naud et al. 2014). Model output or observations are projected onto this grid for each 6-hourly cyclone detected in the model or with reanalysis, and the composite shows the average of all cyclones calculated by superimposing the centers on top of each other. Here we composite total cloud cover, precipitable water (PW), and 500-hPa vertical velocity. For this study, the cyclone-centered composites have been flipped to place the polar side of the cyclones at the top of the figure. We acknowledge that this is a Northern Hemisphere-centric approach.

The cold-front-centered composite grid is assumed to be perpendicular to the surface front, of 100-km horizontal and 1-km vertical resolution for both the observations and the model output (to accommodate for the coarser resolution of the model levels aloft), extends ± 1500 km along the horizontal (the zero point is anchored on the surface front), and spans a 15-km vertical extent above sea level (Naud et al. 2015). The observations are sparse in the cold-frontal region, so we collect any *CloudSat* footprint that is found within a region 3000 km wide (i.e., within 1500 km of the front) and of the cold-front length [see Naud et al. (2015) for more details on the method]. The distance between the profiles and the surface front is used to allocate the *CloudSat*/*CALIPSO* cloud mask profile to a given composite grid box. Some *CloudSat* orbits might intersect the cold front, but this is not a necessary condition. For the model output, the vertical cloud cover profiles are also collected in the 3000-km-wide box centered on the cold front and allocated to the composite grid in the same fashion as the observations. The difference is that all profiles in the box are used for the model composites, while the observations are only available along the *CloudSat* orbit. Another condition that is applied to both observations and model output is that the cloud profile must be outside a 500-km-radius region centered on the low pressure minimum of the parent cyclone to avoid contamination by the wrap-around region and occluded quadrant. The model output that are also composited in these cold-front-centered

transects are the relative humidity and the temperature tendencies for convection.

3. Comparison between modeled and observed cloud cover

The cloud cover comparison is performed for three separate points of view: large scale for the entire ocean basin, at the scale of extratropical cyclones, and at the scale of cold-frontal regions.

a. Large-scale cloud cover and cloud radiative effect in the southern oceans

As a preliminary test, we evaluate the total annual mean cloud cover in the southern oceans produced by the two versions of the model. For reference, we use a 5-yr mean of MODIS monthly observations for 2008–12. In addition, we use CERES longwave and shortwave cloud radiative effect (CRE) estimates to evaluate the CRE from both model versions. According to MODIS retrievals, cloud cover is greater than 85% over the southern oceans between 44° and 64°S, with a thinner band of cloud cover exceeding 95% south of 50°S (Fig. 1a). This is consistent with a longer period of MODIS observations and another instrument (Naud et al. 2014). Both versions of the model also find a relative maximum at these latitudes, but 2PM is negatively biased (too low) by about 5% (Fig. 1b) while MPM is positively biased (too high), also by about 5% (Fig. 1c). While the two versions of the model are fairly close to observations (and actually within observational uncertainties, cf. Naud et al. 2014), they differ from one another by a much larger amount than their individual departure from observations.

The implication of these differences can be examined with the longwave and shortwave cloud radiative effect (Fig. 2). Both model versions tend to predict a larger magnitude of the SW CRE than what is produced with CERES (Fig. 2a), with a larger bias for 2PM (Fig. 2c vs Fig. 2e). This suggests that the modeled clouds are optically thicker than observed, and that 2PM clouds are optically thicker than MPM clouds to compensate for the lower cloud cover. In contrast, both models predict a lower magnitude of the LW CRE than observed with CERES (Fig. 2b), but MPM is closer to the observations than 2PM (Fig. 2f vs Fig. 2d). This suggests that the additional clouds produced with MPM that give larger cloud cover than both 2PM and MODIS are high-level clouds that are optically thin. This is also suggested by the direct comparison of MPM and 2PM SW and LW CRE (Figs. 2g,h).

Because the area of large cloud cover is strongly impacted by extratropical cyclones (Bodas-Salcedo et al.

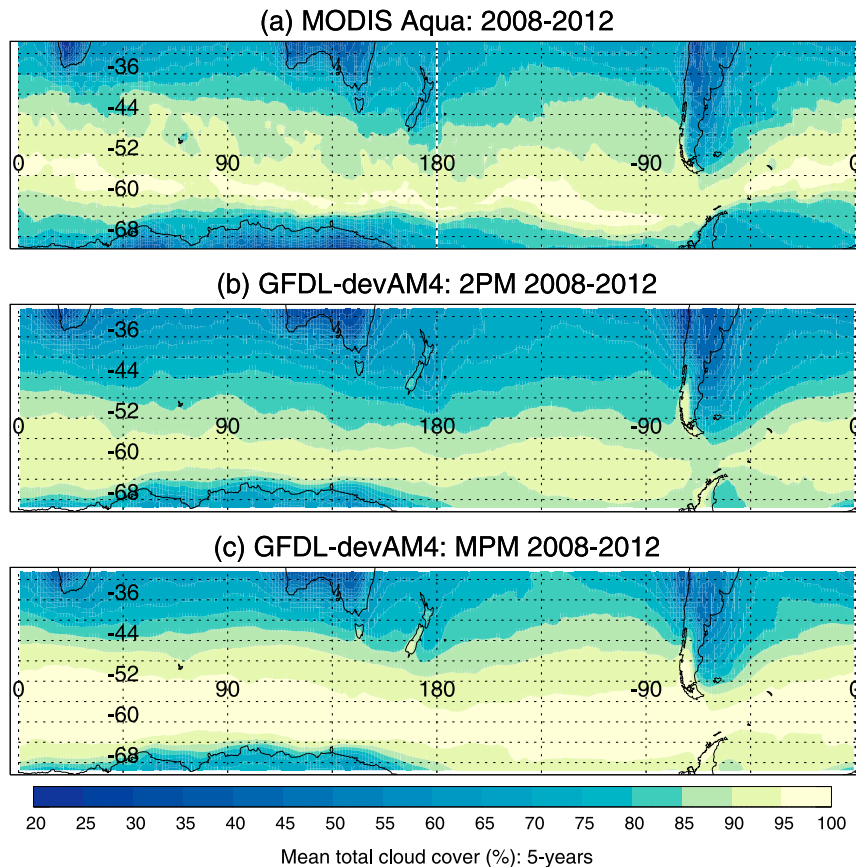


FIG. 1. The 5-yr mean total cloud cover for (a) MODIS, (b) devAM4-2PM, and (c) devAM4-MPM over the Southern Hemisphere midlatitudes for 2008–12, including all months.

2014; Naud et al. 2014), next we focus our attention to the representation of clouds in these systems, and specifically during the warm season (November–March) when the surface shortwave absorption bias is identified (Bodas-Salcedo et al. 2014).

b. Cyclone-centered composites of cloud, precipitable water, and vertical velocity

Cyclone-centered composites are constructed for total cloud cover, PW, and 500-hPa vertical velocities. We remind the reader that the cyclones have been flipped so that the polar side is at the top of the figures. We compare the two model versions to MODIS for total cloud cover and to MERRA-2 for both PW and vertical velocities (Fig. 3).

The cyclone-centered composite of MODIS total cloud cover indicates an area of relatively large cloud cover near the storm center, with decreasing cloud cover into the equator side of the center (Fig. 3a). Both versions of the model give a similar spatial distribution, but also suggest that the maximum near the center has larger cloud cover in the model than observed (Figs. 3b,c). The relative

minimum in the western-equatorward quadrant reveals lower cloud cover for 2PM than observed (Fig. 3b), but larger than observed for MPM (Fig. 3c). This suggests that 1) to be consistent with Figs. 1 and 2 the larger spatial extent of the region of negative bias in 2PM outweighs the region of positive bias near the center and 2) the biases found in Fig. 1 might be related to the biases in the western-equatorward quadrant, which we refer to as the post-cold frontal region (e.g., Naud et al. 2016). The distribution of PW in the cyclones is typically larger on the equator than polar side of the cyclones, and shows a comma-like structure, coinciding with the region of warm air (i.e., the warm sector), with a maximum in the eastern-equatorward quadrant (Figs. 3d–f). There are great similarities between MERRA-2 (Fig. 3d) and both model versions, with MPM slightly drier in the warm sector (Fig. 3f) than MERRA-2 or 2PM. Last, 500-hPa vertical velocities indicate a comma-shaped region of strong ascent to the east of the low and a region of subsidence to the west (Figs. 3g–i), and both model versions agree with MERRA-2 distribution. This said, the ascent appears to be stronger in the two versions of the model than in MERRA-2.

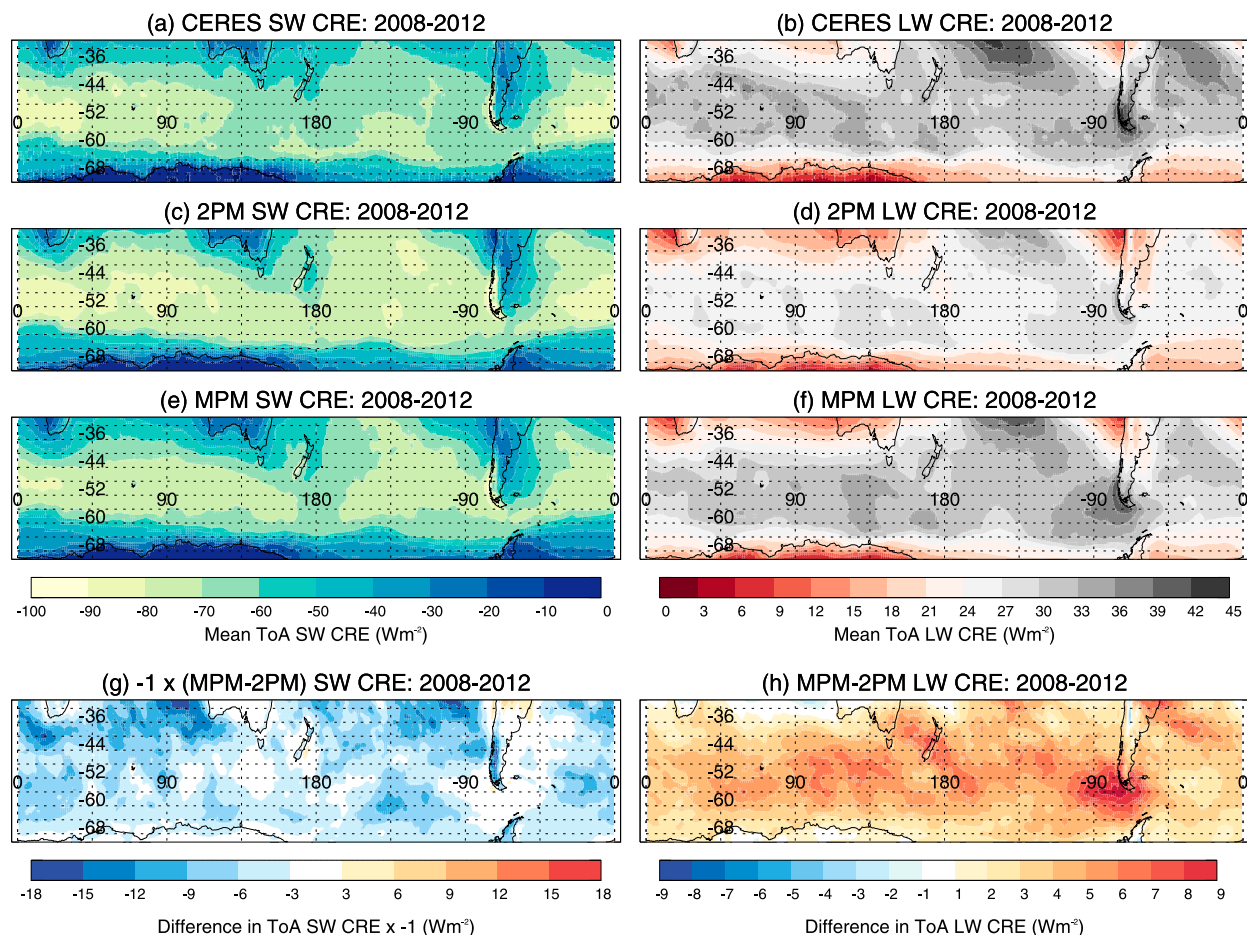


FIG. 2. The 5-yr mean cloud radiative effect for (a) CERES shortwave, (b) CERES longwave, (c) devAM4-2PM SW, (d) devAM4-2PM LW, (e) devAM4-MPM SW, and (f) devAM4-MP LW over the Southern Hemisphere midlatitudes for 2008–12, including all months. Also shown is the difference between devAM4-MPM and devAM4-2PM (g) SW CRE and (h) LW CRE.

To quantify the differences between the models and observations/reanalysis, we examine composite differences (Fig. 4). Both model versions produce a larger cloud cover than observed near the center of the cyclone into the warm sector, with differences around 5% for 2PM (Fig. 4a) and 10% for MPM (Fig. 4b). This might be related to the stronger ascent in devAM4 compared to MERRA2 (Figs. 4e,f). However, the two versions show different cloud cover biases in the western-equatorward quadrant, with a low bias for 2PM (up to 7%) and a slightly positive bias for MPM (under 5%). This cannot be explained by differences with MERRA-2 in PW (Figs. 4c,d) as these are less than 0.5 mm or of a sign opposite to the cloud cover bias, or by differences in the dynamics, again near zero in this quadrant (Figs. 4e,f). Overall, the differences in cloud cover indicate a contrast between the western and eastern equatorward quadrants of the cyclones.

To obtain more details on the differences we find in the equatorward half of the cyclone region between the

two model versions and observations, we next turn to composites across cold fronts and *CloudSat/CALIPSO* observations: this will help determine which cloud level might cause the total cloud cover differences, and analyze the biases with respect to the location of the cold front.

c. Cold-frontal transects of cloud cover

Here we examine how clouds are distributed vertically on both sides of the cold fronts. The observations are provided by *CloudSat/CALIPSO* (Fig. 5a). The observations indicate that on the west side of the surface front (i.e., the post-cold frontal region), low-level clouds dominate (<3 km), and occur up to 44% of the time (Fig. 5a). Mid- and high-level clouds occur less than 20% of the time [consistent with Naud et al. (2015, 2018)]. On the eastern side of the front (i.e., the warm sector), clouds occur at all altitudes (from 0 to ~12 km) 30%–40% of the time as this is the region of the warm conveyor belt [as defined by Browning (1986)].

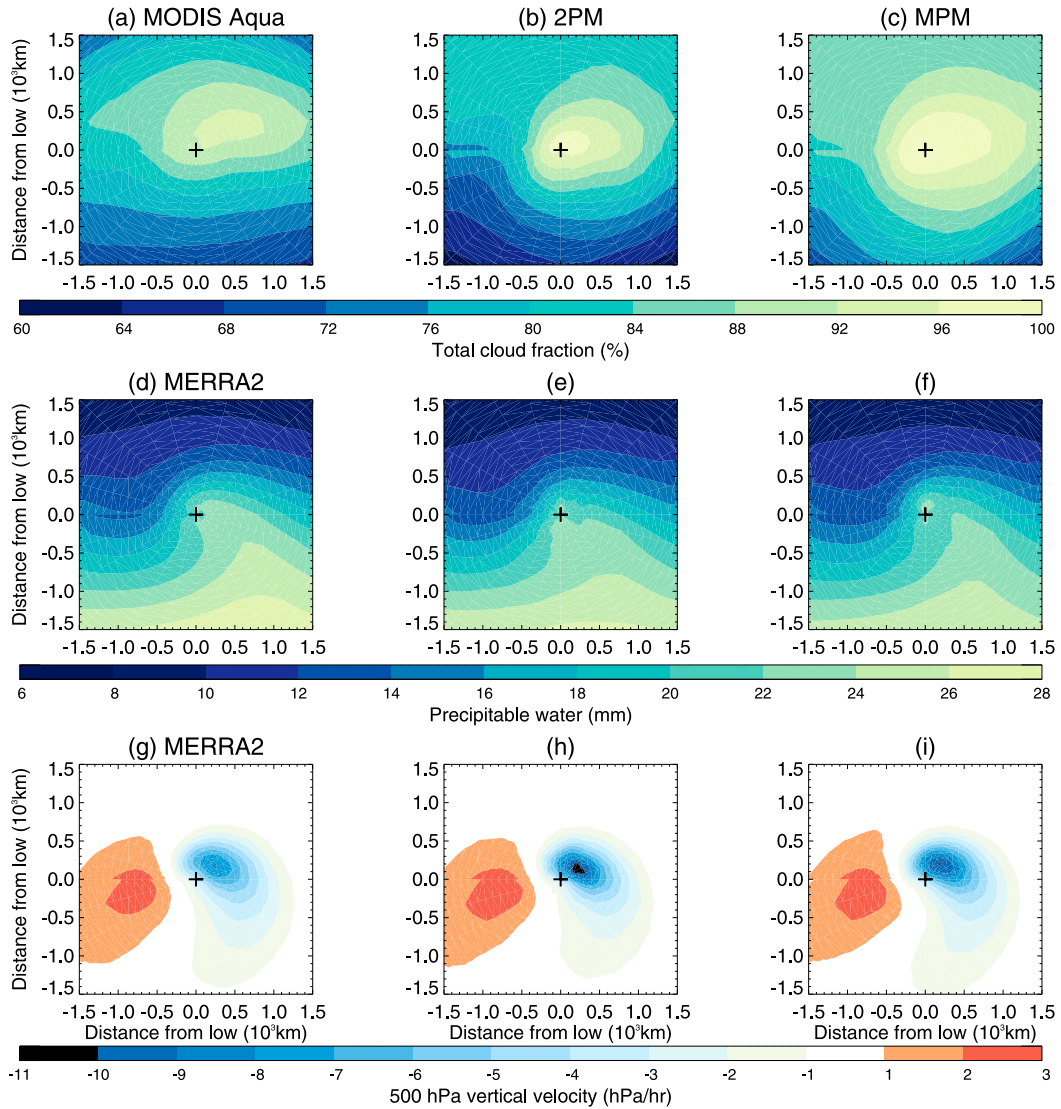


FIG. 3. Cyclone-centered composites of (top) total cloud cover, (middle) PW, and (bottom) 500-hPa vertical velocities from (a) MODIS, (d),(g) MERRA-2, (b),(e),(h) 2PM, and (c),(f),(i) MPM for SH cyclones in November–March.

Both model versions show a similar spatial distribution of cloud as observed across the entire cold-frontal region (Figs. 5b,c). However, both underestimate low-level cloud cover in the post-cold frontal region by 10%–20% and slightly overestimate mid- and high-level cloud cover by 4%–8%. In the warm sector, both versions predict cloud cover similar to the observations, albeit with a low bias of 10%–20% at middle and low levels and a tendency to predict more high-level clouds (at least +10%).

The differences between the model and the observations above 5 km (i.e., greater modeled cloud cover than observed) can help to explain the differences found when comparing with MODIS (Fig. 4). A top-down view

would indeed indicate greater total cloud cover in the model than observed based on differences at high and midlevels regardless of potential deficiency in low-level clouds. However, there are clear differences between the two model versions: MPM predicts a larger cloud cover at low levels in the post-cold frontal region and tends to predict high-level cloud cover at higher altitudes in the warm sector (Fig. 5c), with fewer midlevel clouds than 2PM (Fig. 5b). These differences, and those highlighted when comparing with MODIS observations, suggest that the representation of convection has implications for the correct representation of cloud in extratropical cyclones, and more specifically in cold-frontal regions. However, it is unclear how much

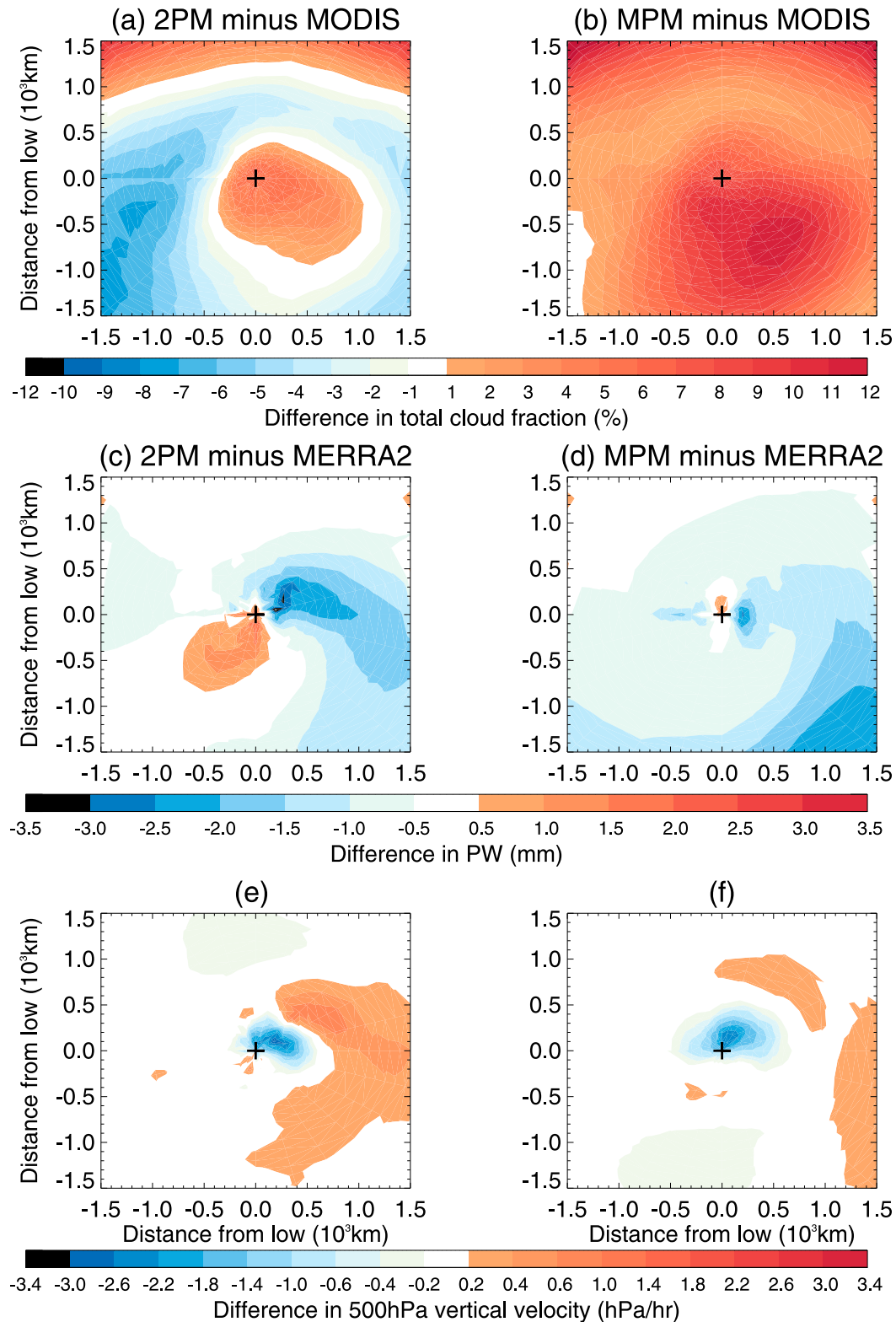


FIG. 4. Difference in cyclone-centered composites of (a),(b) cloud cover, (c),(d) PW, and (e),(f) 500-hPa vertical velocities between (left) 2PM or (right) MPM and MODIS [in (a) and (b)] or MERRA2 for SH cyclones in November–March.

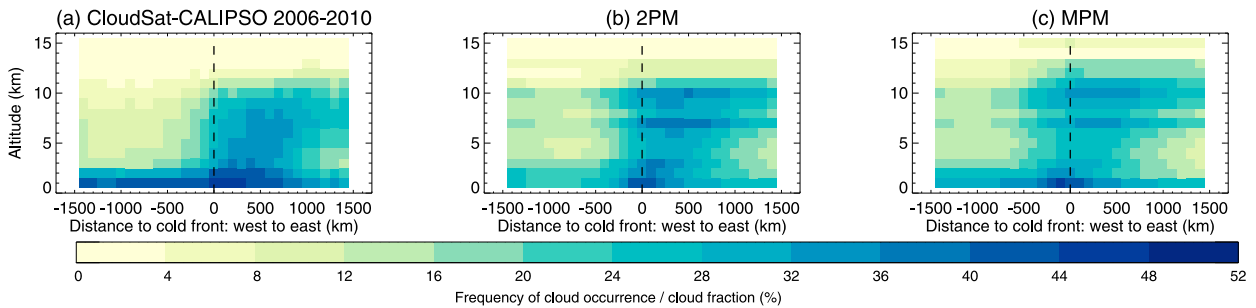


FIG. 5. Cold-front-centered composites of vertical cloud distribution from (a) *CloudSat*/*CALIPSO* averaged over 2006–16, (b) as modeled with devAM4 2PM, and (c) as modeled with devAM4-MPM. The vertical dashed line indicates the location of the surface front: the post-cold frontal or cold side of the front is to the left of this line, and the pre-cold frontal or warm side of the front is to the right. These are Southern Hemisphere cold fronts during November–March.

cloud-parameter tuning differences participate in these differences. So next we explore in more detail the differences between 2PM and MPM to help better understand how convection parameterizations and tuning impact cloud cover in these regions.

4. Discussion

The two model versions exhibit cloud differences that are not uniform across the cold-frontal region, with 1) larger cloud cover in MPM above 10 km on both sides of the front, 2) lower cloud cover in MPM than 2PM in the warm sector from the surface to 10 km, and 3) larger cloud cover in MPM in the post-cold frontal region at all altitudes, mostly in a region between 100 and 1000 km to the west of the front (Fig. 5). When distinguishing cloud cover produced with the large-scale cloud scheme (Fig. 6a) from the cloud cover directly produced by the convection scheme (Fig. 6b), it appears that large-scale cloud cover dominates, with cloud cover from convection occurring less than 2% of the time. Differences between the two model versions are thus dominated by differences in the large-scale cloud scheme (Fig. 6d). The convection scheme still plays an important role in forming the total cloud, because it acts as a source and sink for cloud condensate for the large-scale scheme. We also note that while convective cloud fractions are small, the relative differences in convective cloud cover are large between the two model versions (Fig. 6e vs Fig. 6b). Therefore, we will use this discussion to explain how the cloud differences, both the large-scale and convective cloud, relate to differences in the parameterizations and differences in the tuning parameters (detailed in section 2, and Table 2).

a. Differences above 10 km

Above 10 km, MPM has more large-scale and convective cloud than 2PM all across the cold-frontal transect

(pre- and postfrontal zones) (Figs. 6d,e), and the same difference occurs for RH (Fig. 6f). The larger RH in MPM is most likely a result of deeper convection in MPM than 2PM: temperature tendencies from convection are greater above 10 km in MPM than 2PM (Fig. 7) and the maximum height of convective plumes is also higher in MPM than 2PM (Fig. 8). This increased convection would lead to higher RH, and therefore more clouds above 10 km in MPM than 2PM (Fig. 5). However, another factor impacting clouds at this height is the lower ice crystal fall speeds in the large-scale cloud scheme in the MPM model version. All of the clouds at this height are ice clouds, and the lower fall speeds means that MPM has a weaker cloud sink than 2PM.

The relative impact of the convection scheme and tuning depends on the model base state. When we change the tuning in 2PM, i.e., 2PM (MPM Tune), and compare large-scale cloud cover with MPM, the effect of the change in convection scheme is significant above 10 km (Fig. 6g). However, if the change in convection scheme is applied to a model with 2PM tuning [i.e., MPM (2PM Tune) vs 2PM] while the difference above 10 km is still visible, its magnitude is much smaller (Fig. 6p), presumably because the amount of ice at upper levels is depleted more rapidly with the 2PM crystal fall speed. Conversely, the impact of the ice crystal fall speed change is much greater when applied to MPM than 2PM (Fig. 6m vs Fig. 6j), presumably because the change affects a larger amount of ice in MPM than 2PM above 10 km because of deeper convection in MPM.

b. Differences below 10 km: Postfrontal region

Below 10 km, extending down to the surface, MPM has more large-scale cloud than 2PM in the post-cold frontal region (Fig. 6d). The differences in convective cloud do not mimic the differences in large-scale cloud (Fig. 6e), and even more surprisingly the RH differences in the post-cold frontal region do not match the cloud

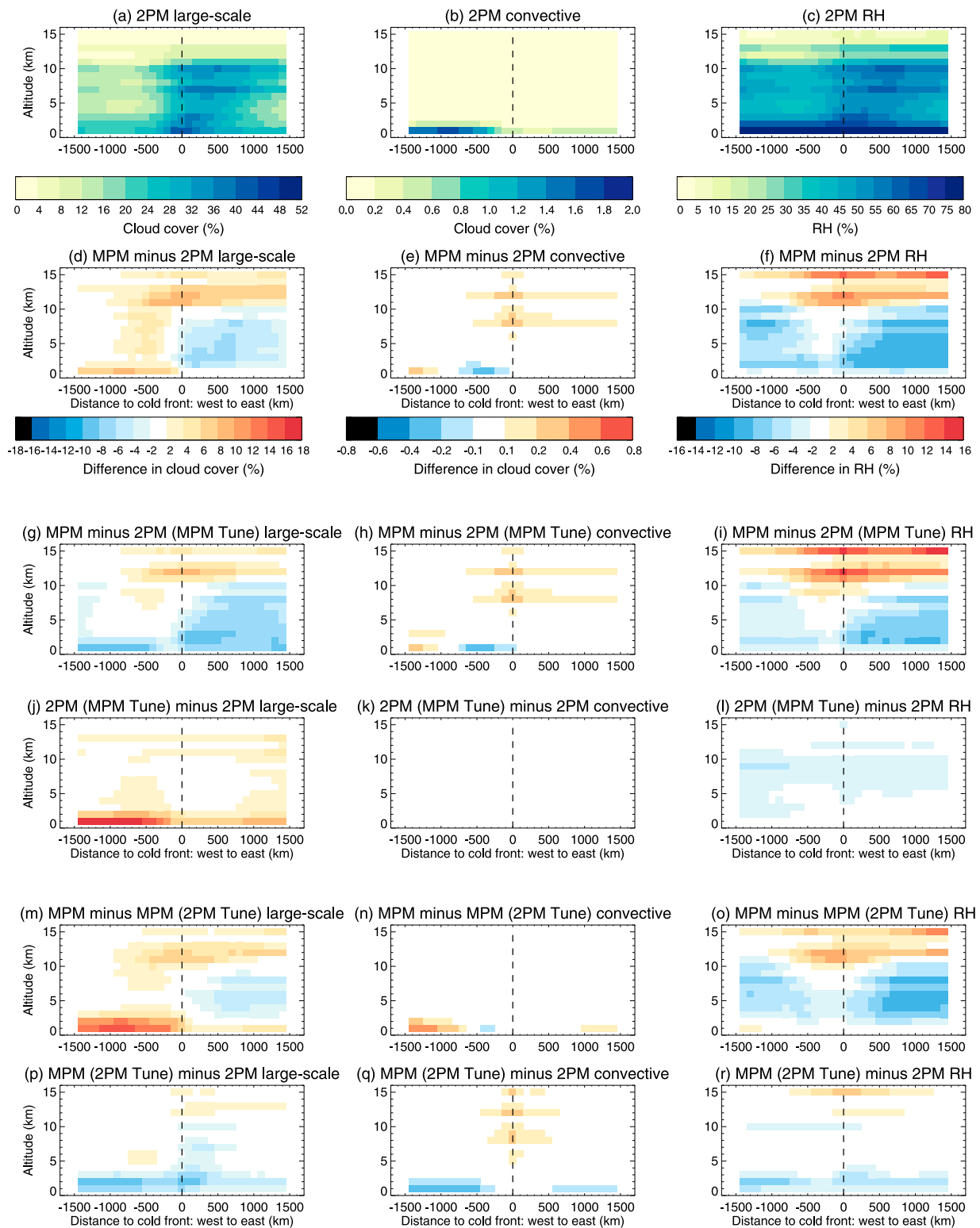


FIG. 6. Cold-front-centered composites of the 2PM (a) large-scale and (b) convective cloud cover and (c) RH, and difference in large-scale cloud cover, convective cloud cover, and RH between the following pairs: (d)–(f) MPM and 2PM, (g)–(i) MPM and 2PM (MPM Tune), (j)–(l) 2PM (MPM Tune) and 2PM, (m)–(o); MPM and MPM (2PM Tune), and (p)–(r) MPM (2PM Tune) and 2PM. The vertical dashed line indicates the location of the surface front; the post-cold frontal or cold side of the front is to the left of this line, and the pre-cold frontal or warm side of the front is to the right. These are Southern Hemisphere cold fronts during November–March.

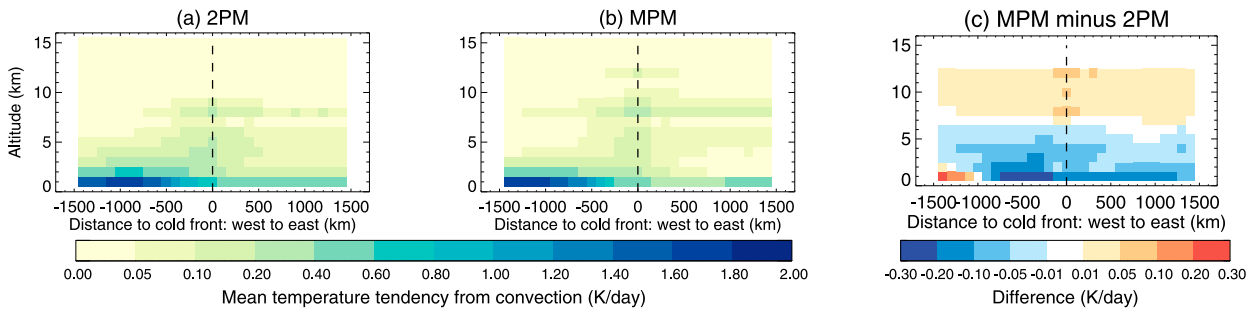


FIG. 7. Cold-front-centered composites of temperature tendencies for convection from (a) 2PM and (b) MPM, and (c) the difference between MPM and 2PM. The vertical dashed line indicates the location of the surface front; the post-cold frontal or cold side of the front is to the left of this line, and the pre-cold frontal or warm side of the front is to the right. These are Southern Hemisphere cold fronts during November–March.

differences (Fig. 6f). Thus, MPM has more large-scale cloud but lower RH in the post-cold frontal zone, as compared to 2PM. These seemingly contrasting differences are most likely related to differences in the cloud sinks for the two configurations. The higher amount of large-scale cloud in MPM is consistent with a larger volume-mean drop radius for precipitation in the MPM large-scale cloud scheme (see discussion for precipitation in section 4d). The lower amount of large-scale cloud and higher RH in 2PM is consistent with a more rapid erosion of the large-scale clouds in 2PM. By imposing a larger volume-mean drop radius for precipitation and a slower erosion in 2PM (MPM Tune), greater large-scale cloud cover than in the original 2PM post-cold frontal region is produced (Fig. 6j). This also means that for the same set of tuning parameters the 2PM model produces in fact larger cloud cover below 3 km in the post-cold frontal region than MPM (Figs. 6g or 6p). In contrast, the MPM convective cloud cover in this area is mostly lower than for 2PM, and it seems to be dominated by the change in convection scheme (e.g., Fig. 6h vs Fig. 6k). This said, again the order in which the

tuning and convection scheme are changed matters (Figs. 6n and 6q vs Figs. 6h and 6k).

c. Differences below 10 km: Prefrontal region

In the prefrontal region below 10 km, the situation is less complicated. MPM large-scale cloud cover and RH are both lower than 2PM cloud and RH (Figs. 6d,f). Moreover, the lower RH in MPM negates the impact of erosion and volume-mean drop radius tuning parameters that cause greater large-scale cloud cover below 2 km for both MPM and 2PM convection schemes (Figs. 6j,m).

d. The relation between cloud and precipitation differences

Precipitation is a sink of moisture, and while MPM is tuned to have a greater precipitation efficiency parameter than 2PM for shallow convection, the treatments for convective microphysics in deep convection are structured differently in MPM and 2PM. This might help retain slightly more convective condensate in the lowest 5 km above the surface in MPM than in 2PM that can

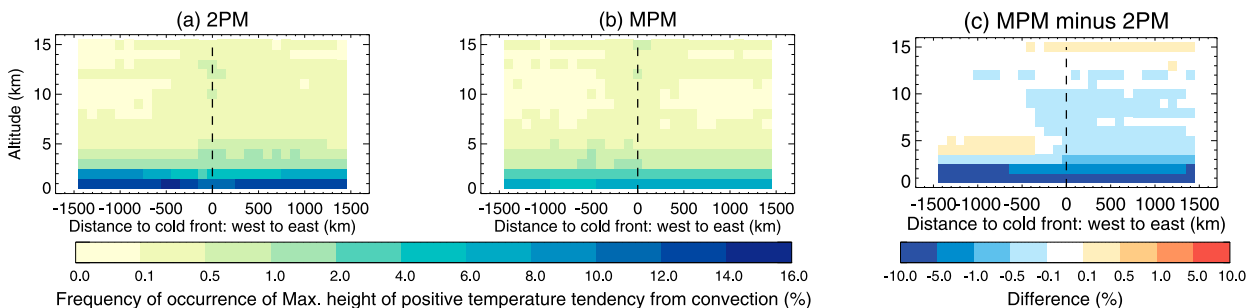


FIG. 8. Cold-front transect vertical distribution of the maximum height of the convective column in (a) 2PM and (b) MPM, and (c) difference in height between MPM and 2PM. The vertical dashed line indicates the location of the surface front; the post-cold frontal or cold side of the front is to the left of this line, and the pre-cold frontal or warm side of the front is to the right. These are Southern Hemisphere cold fronts during November–March.

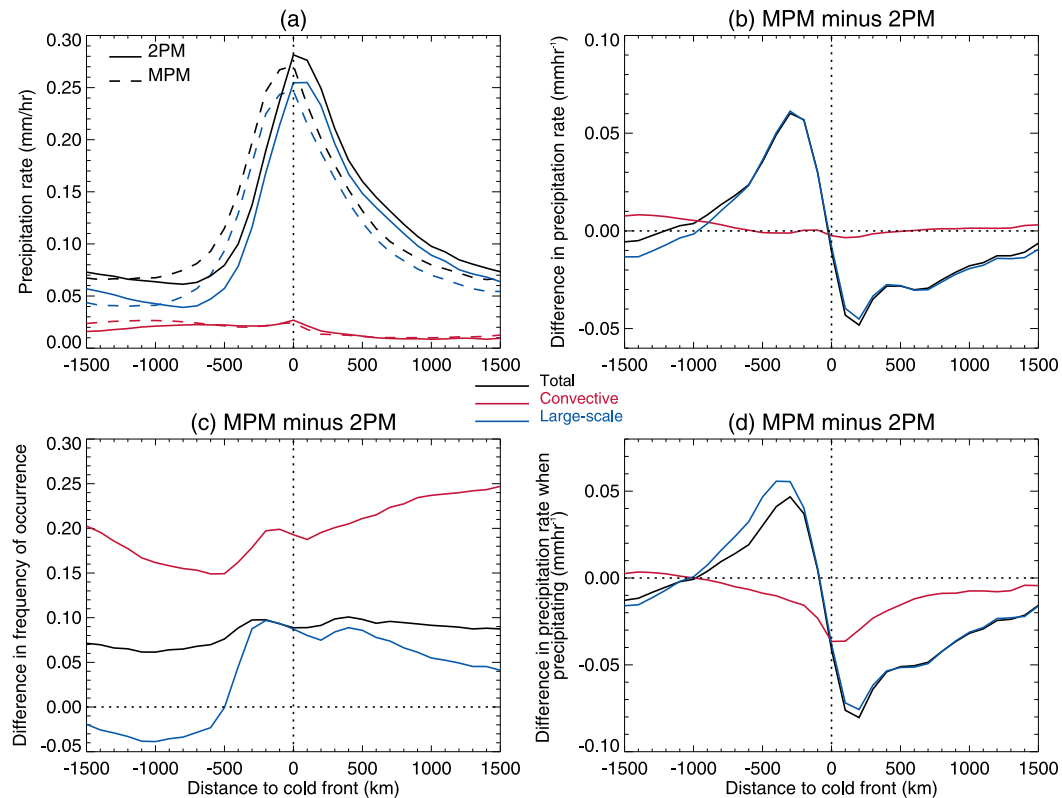


FIG. 9. Cold-front-centered composite of (a) mean precipitation for 2PM (solid) and MPM (dashed) for total (black), convective (red), and large-scale (blue) precipitation and difference between MPM and 2PM in (b) mean precipitation, (c) frequency of precipitation, and (d) precipitation rate when precipitating. The vertical dashed line indicates the location of the surface front; the post-cold frontal or cold side of the front is to the left of this line, and the pre-cold frontal or warm side of the front is to the right. These are Southern Hemisphere cold fronts during November–March.

then be passed on to the large-scale cloud scheme. In nature, precipitation rates are low in post-cold frontal regions (Naud et al. 2015) and both model versions tend to represent this fairly well (Fig. 9a). MPM tends to predict larger precipitation rates than 2PM in the post-cold frontal region but lower precipitation in the warm sector (Fig. 9b), with greater differences in the large-scale than convective precipitation. In fact, while MPM produces convective precipitation more often than 2PM (Fig. 9c), in accordance with a greater shallow convective precipitation efficiency, it also produces lower convective precipitation rates than 2PM (Fig. 9d), which helps to keep the difference in total convective precipitation close to zero (Fig. 9b). Therefore, the sink that convective precipitation could be is somewhat similar between the two model versions, with compensating effect of frequency of occurrence and rates when precipitating. In the post-cold frontal region, while MPM tends to produce more large-scale precipitation overall (Fig. 9a), it is because the precipitation rates when precipitating (i.e., intensity) are larger than for 2PM

(Fig. 9d). In fact, large-scale precipitation occurs more often in 2PM (Fig. 9c) which could explain the paradox of larger precipitation and cloud cover in MPM. This may be explained by the impact of a larger volume-mean drop radius threshold for MPM to precipitate, so that when it does precipitate in MPM the intensity is greater (Fig. 9d).

5. Conclusions

Using MODIS, *CloudSat*, and *CALIPSO* observations of cloud cover in extratropical cyclones and cold-frontal regions, a recent development version of the GFDL AM4 model (Zhao et al. 2018a,b) is evaluated for two different versions of the convection scheme. One version, referred to as 2PM, is a two-plume model that uses the Bretherton et al. (2004) convection scheme for both shallow and deep convection (Zhao et al. 2018b). The other scheme, referred to as MPM, is a multiplume model that handles shallow convection with the same scheme but handles deep convection with the Donner

et al. (2001) scheme. Both models predict realistic monthly cloud cover over the Southern Oceans when compared with MODIS, but 2PM predicts about 10% less cloud cover than MPM (i.e., a difference between the two model versions greater than their respective deviation from observations). While MPM shortwave and longwave cloud radiative effects are quite close to observations, 2PM tends to exhibit larger magnitude in shortwave cloud radiative effect but lower magnitude in the longwave. This suggests that while MPM might produce greater cloud coverage, 2PM tends to produce optically thicker clouds, and overall lower cloud-top heights. A similar discrepancy in cloud cover between the two models and with observations is found in the cold sector of extratropical cyclones, and more specifically in cold-frontal regions.

A closer examination of cloud vertical profiles in these cold-frontal regions reveals that both model versions overestimate cloud cover at high levels (i.e., above 10 km) but underestimate cloud cover at low and mid-levels. In the warm sector of the cyclone, this altitude-dependent bias is larger for MPM, and is easily explained when examining differences in relative humidity profiles. Both model versions are top-heavy for both convective and large-scale cloud fraction, and more so in the warm sector and when using the MPM scheme.

In the post-cold frontal regions, both model versions underestimate low-level cloud cover but the bias is larger for 2PM. This area of negative bias is in fact the area where convective activity is largest in the entire cold-frontal region for both model versions. The convective activity at low levels in the post-cold frontal region is larger but shallower in 2PM than MPM. Because convective cloud cover is much smaller than cloud cover predicted with the large-scale cloud scheme, the convection parameterizations are either too efficient at precipitating or not efficient enough at detraining condensate. These efficiencies are controlled by parameters that can be tuned in the model. Convective detrainment above the boundary layer, lateral mixing effects, stratiform cloud erosion, and precipitation efficiency are different between the two model versions, and these differences are contributing to the discrepancies we have found. In fact, the choices made for the MPM tuning tend to help maintain cloud in the post-cold frontal region. Overall, it seems that both model versions might just be too convectively active, thus preventing the large-scale cloud scheme to be called often enough. This problem was found in stratocumulus cloud regions in a more recent version of the model and corrections have been put in place (Zhao et al. 2018b). Zhao et al. (2018b) report issues in the full AM4.0 regarding unrealistically large shallow convective activity

in regions of stratocumulus clouds that can cause an underestimate in low-level cloud cover. This problem would also be present in these devAM4 versions. In the released AM4.0 version of this model, this overactivity is counteracted by forcing the model to switch off the convection scheme in favor of the large-scale cloud scheme when the Wood and Bretherton (2006) EIS parameter exceeds 8 K. In Naud et al. (2016), post-cold frontal regions were found to exhibit values of EIS much lower than 8 K so it is not clear at this point whether this correction will help predict values of cloud cover in post-cold frontal region closer to the 40%–45% indicated by *CloudSat/CALIPSO* observations.

It remains that the relatively more active convection in the post-cold frontal boundary layer is somewhat inhibiting the formation and persistence of clouds in devAM4. However, it appears that tuning plays a significant role. This suggests that while cumulus parameterization is playing a role in the current models difficulties to reproduce a realistic cloud cover in the cold sector of extratropical cyclones, it cannot be excluded as well that both model versions are correct to be so convectively active in this region. If this is the case then our analysis implies that both convection schemes do not produce enough clouds, and that this might be because of tuning choices.

Despite the numerous differences between extratropical cyclone clouds in the two models, the differences between the low-level, post-cold frontal clouds in either model and *CloudSat* are substantially larger. Presumably, this bias is related to the fact that both models have too much upper-level cloud in the post-cold frontal region; however, cause and effect for these two issues are hard to discern. The fact that the differences between the two models did not significantly impact these biases points to a need to consider other model physics, such as parameterized vertical transport in the boundary layer. Furthermore, the physics differences between the two configurations compared for this paper are of a similar magnitude as the differences between devAM4 and AM4. Therefore, we cannot expect AM4 to have completely removed the bias in low-level clouds shown here. However, the changes made for AM4, such as removing total condensate as precipitation separately for liquid and ice phase clouds and adding a threshold related to EIS, may contribute to a reduction in the bias.

One goal of this study was to evaluate how sensitive post-cold frontal cloud cover might be to the way convection is parameterized. Doing so in a GCM requires a fine balance between applying substantial changes and maintaining a realistic climate. Therefore the choice of tuning parameters (used for the cloud parameterization)

also has a significant impact on the results. While changes in convection scheme and these tuning parameters appear to be additive and lead together to similar output, the same tuning applied to differing model base states can have different effects. Although this is found for a specific model, this should apply to most current climate models of similar resolution. This is because a number of parameters need to be set in cloud parameterizations, and not all are observable, or observations are either scarce or highly uncertain (e.g., Hourdin et al. 2017; Schmidt et al. 2017).

Nevertheless, the work presents a framework that might guide further model development, on convection parameterization as well as other aspects of the model. Moreover, once these cold-front-oriented metrics that were developed here can be automated, which is anticipated to be completed in late 2019, modeling centers can use these diagnostics in line with development.

Acknowledgments. This research is funded by NOAA MAP Grant NA15OAR4310094. CMN received additional support from the NASA MAP Grant 80NSSC17K0195. The MCMS algorithm and documentation can be found online (<http://gcss-dime.giss.nasa.gov/mcms>). The database of cold fronts is available online (<http://portal.nccs.nasa.gov/datashare/Obs-ETC/Fronts-ETC/>). The MODIS files were obtained through the LAADS DAAC (<http://ladsweb.modaps.eosdis.nasa.gov>), the *CloudSat/CALIPSO* GEOPROF-LIDAR files were obtained through the *CloudSat* data processing center (<http://www.cloudsat.cira.colostate.edu>), the MERRA-2 products come from NASA Goddard Earth Sciences Data and Information Services Center, and the ERA-Interim products are from the European Centre for Medium-Range Weather Forecasts Internet site.

REFERENCES

- Ackerman, S. A., R. E. Holz, R. Frey, E. W. Eloranta, B. C. Maddux, and M. McGill, 2008: Cloud detection with MODIS. Part II: Validation. *J. Atmos. Oceanic Technol.*, **25**, 1073–1086, <https://doi.org/10.1175/2007JTECHA1053.1>.
- Bauer, M., and A. D. Del Genio, 2006: Composite analysis of winter cyclones in a GCM: Influence on climatological humidity. *J. Climate*, **19**, 1652–1672, <https://doi.org/10.1175/JCLI3690.1>.
- , G. Tselioudis, and W. B. Rossow, 2016: A new climatology for investigating storm influences in and on the extratropics. *J. Appl. Meteor. Climatol.*, **55**, 1287–1303, <https://doi.org/10.1175/JAMC-D-15-0245.1>.
- Bodas-Salcedo, A., and Coauthors, 2011: COSP: Satellite simulation software for model assessment. *Bull. Amer. Meteor. Soc.*, **92**, 1023–1043, <https://doi.org/10.1175/2011BAMS2856.1>.
- , K. D. Williams, P. R. Field, and A. P. Lock, 2012: The surface downwelling solar radiation surplus over the Southern Ocean in the Met Office Model: The role of midlatitude cyclone clouds. *J. Climate*, **25**, 7467–7486, <https://doi.org/10.1175/JCLI-D-11-00702.1>.
- , and Coauthors, 2014: Origins of the solar radiation biases over the Southern Ocean in CFMIP2 models. *J. Climate*, **27**, 41–56, <https://doi.org/10.1175/JCLI-D-13-00169.1>.
- Booth, J. F., C. M. Naud, and A. D. Del Genio, 2013: Diagnosing warm frontal cloud formation in a GCM: A novel approach using conditional subsetting. *J. Climate*, **26**, 5827–5845, <https://doi.org/10.1175/JCLI-D-12-00637.1>.
- Bretherton, C. S., J. R. McCaa, and H. Grenier, 2004: A new parameterization for shallow cumulus convection and its application to marine subtropical cloud-topped boundary layers. Part I: Description and 1D results. *Mon. Wea. Rev.*, **132**, 864–882, [https://doi.org/10.1175/1520-0493\(2004\)132<0864:ANPFSC>2.0.CO;2](https://doi.org/10.1175/1520-0493(2004)132<0864:ANPFSC>2.0.CO;2).
- Browning, K. A., 1986: Conceptual models of precipitation systems. *Wea. Forecasting*, **1**, 23–41, [https://doi.org/10.1175/1520-0434\(1986\)001<0023:CMOPS>2.0.CO;2](https://doi.org/10.1175/1520-0434(1986)001<0023:CMOPS>2.0.CO;2).
- Ceppi, P., and D. L. Hartmann, 2016: Clouds and the atmospheric circulation response to warming. *J. Climate*, **29**, 783–799, <https://doi.org/10.1175/JCLI-D-15-0394.1>.
- Dee, D. P., and Coauthors, 2011: The ERA-Interim reanalysis: Configuration and performance of the data assimilation systems. *Quart. J. Roy. Meteor. Soc.*, **137**, 553–597, <https://doi.org/10.1002/qj.828>.
- Donner, L. J., C. Seman, R. Hemler, and S.-M. Fan, 2001: A cumulus parameterization including mass fluxes, convective vertical velocities, and mesoscale effects. *J. Climate*, **14**, 3444–3463, [https://doi.org/10.1175/1520-0442\(2001\)014<3444:ACPIMF>2.0.CO;2](https://doi.org/10.1175/1520-0442(2001)014<3444:ACPIMF>2.0.CO;2).
- , and Coauthors, 2011: The dynamical core, physical parameterizations, and basic simulation characteristics of the atmospheric component AM3 of the GFDL global coupled model CM3. *J. Climate*, **24**, 3484–3519, <https://doi.org/10.1175/2011JCLI3955.1>.
- Field, P. R., A. Gettelman, R. Neale, R. Wood, P. J. Rasch, and H. Morrison, 2008: Midlatitude cyclone compositing to constrain climate model behavior using satellite observations. *J. Climate*, **21**, 5887–5903, <https://doi.org/10.1175/2008JCLI2235.1>.
- , A. Bodas-Salcedo, and M. E. Brooks, 2011: Using model analysis and satellite data to assess cloud and precipitation in midlatitude cyclones. *Quart. J. Roy. Meteor. Soc.*, **137**, 1501–1515, <https://doi.org/10.1002/qj.858>.
- Frey, W. R., and J. E. Kay, 2018: The influence of extratropical cloud phase and amount feedbacks on climate sensitivity. *Climate Dyn.*, **50**, 3097–3116, <https://doi.org/10.1007/s00382-017-3796-5>.
- Gelaro, R., and Coauthors, 2017: The Modern-Era Retrospective Analysis for Research and Applications, version 2 (MERRA-2). *J. Climate*, **30**, 5419–5454, <https://doi.org/10.1175/JCLI-D-16-0758.1>.
- Golaz, J.-C., L. W. Horowitz, and H. Levy II, 2013: Cloud tuning in a coupled climate model: Impact on 20th century warming. *Geophys. Res. Lett.*, **40**, 2246–2251, <https://doi.org/10.1002/grl.50232>.
- Govekar, P. D., C. Jakob, and J. Catto, 2014: The relationship between clouds and dynamics in Southern Hemisphere extratropical cyclones in the real world and a climate model. *J. Geophys. Res. Atmos.*, **119**, 6609–6628, <https://doi.org/10.1002/2013JD020699>.
- Grise, K. M., and B. Medeiros, 2016: Understanding the varied influence of midlatitude jet position on clouds and cloud radiative effects in observations and global climate models. *J. Climate*, **29**, 9005–9025, <https://doi.org/10.1175/JCLI-D-16-0295.1>.

- Hewson, T. D., 1998: Objective fronts. *Meteor. Appl.*, **5**, 37–65, <https://doi.org/10.1017/S1350482798000553>.
- Hourdin, F., and Coauthors, 2017: The art and science of climate model tuning. *Bull. Amer. Meteor. Soc.*, **98**, 589–602, <https://doi.org/10.1175/BAMS-D-15-00135.1>.
- Kay, J. E., C. Wall, V. Yettella, B. Medeiros, C. Hannay, P. Caldwell, and C. Bitz, 2016: Global climate impacts of fixing the Southern Ocean shortwave radiation bias in the Community Earth System Model (CESM). *J. Climate*, **29**, 4617–4636, <https://doi.org/10.1175/JCLI-D-15-0358.1>.
- Klein, S. A., and C. Jakob, 1999: Validation and sensitivities of frontal clouds simulated by the ECMWF model. *Mon. Wea. Rev.*, **127**, 2514–2531, [https://doi.org/10.1175/1520-0493\(1999\)127<2514:VASOFC>2.0.CO;2](https://doi.org/10.1175/1520-0493(1999)127<2514:VASOFC>2.0.CO;2).
- Lamraoui, F., J. F. Booth, C. M. Naud, M. Jensen, and K. L. Johnson, 2019: The interaction between boundary layer and convection schemes in a WRF simulation of post cold frontal clouds over the ARM East North Atlantic site. *J. Geophys. Res. Atmos.*, **124**, 4699–4721, <https://doi.org/10.1029/2018JD029370>.
- Loeb, N. G., and Coauthors, 2018: Clouds and the Earth's Radiant Energy System (CERES) Energy Balanced and Filled (EBAF) top-of-atmosphere (TOA) edition-4.0 data product. *J. Climate*, **31**, 895–918, <https://doi.org/10.1175/JCLI-D-17-0208.1>.
- Mace, G. G., and Q. Zhang, 2014: The *CloudSat* radar-lidar geometrical profile product (RL-GeoProf): Updates, improvements, and selected results. *J. Geophys. Res. Atmos.*, **119**, 9441–9462, <https://doi.org/10.1002/2013JD021374>.
- Menzel, W. P., and Coauthors, 2008: MODIS global cloud-top pressure and amount estimation: Algorithm description and results. *J. Appl. Meteor. Climatol.*, **47**, 1175–1198, <https://doi.org/10.1175/2007JAMC1705.1>.
- Morrison, A. E., S. T. Siems, and M. J. Manton, 2011: A three-year climatology of cloud-top phase over the Southern Ocean and North Pacific. *J. Climate*, **24**, 2405–2418, <https://doi.org/10.1175/2010JCLI3842.1>.
- Naud, C. M., A. D. Del Genio, M. Bauer, and W. Kovari, 2010: Cloud vertical distribution across warm and cold fronts in *CloudSat*–*CALIPSO* data and a general circulation model. *J. Climate*, **23**, 3397–341, <https://doi.org/10.1175/2010JCLI3282.1>.
- , J. F. Booth, D. J. Posselt, and S. C. van den Heever, 2013: Multiple satellite observations of cloud cover in extratropical cyclones. *J. Geophys. Res.*, **118**, 9982–9996, <https://doi.org/10.1002/JGRD.50718>.
- , —, and A. D. Del Genio, 2014: Evaluation of ERA-Interim and MERRA cloudiness in the Southern Ocean. *J. Climate*, **27**, 2109–2124, <https://doi.org/10.1175/JCLI-D-13-00432.1>.
- , D. J. Posselt, and S. C. van den Heever, 2015: A *CloudSat*–*CALIPSO* view of cloud and precipitation properties across cold fronts over the global oceans. *J. Climate*, **28**, 6743–6762, <https://doi.org/10.1175/JCLI-D-15-0052.1>.
- , J. F. Booth, and A. D. Del Genio, 2016: The relationship between boundary layer stability and cloud cover in the post-cold-frontal region. *J. Climate*, **29**, 8129–8149, <https://doi.org/10.1175/JCLI-D-15-0700.1>.
- , D. J. Posselt, and S. C. van den Heever, 2018: Reply to “Comments on ‘A *CloudSat*–*CALIPSO* view of cloud and precipitation properties across cold fronts over the global oceans.’” *J. Climate*, **31**, 2969–2975, <https://doi.org/10.1175/JCLI-D-17-0777.1>.
- Salomonson, V. V., W. L. Barnes, P. W. Maymon, H. E. Montgomery, and H. Ostrow, 1989: MODIS: Advanced facility instrument for studies of the Earth as a system. *IEEE Trans. Geosci. Remote Sens.*, **27**, 145–153, <https://doi.org/10.1109/36.20292>.
- Schmidt, G. A., and Coauthors, 2017: Practice and philosophy of climate model tuning across six U.S. modeling centers. *Geosci. Model Dev.*, **10**, 3207–3223, <https://doi.org/10.5194/gmd-10-3207-2017>.
- Simmonds, I., K. Keay, and J. A. T. Bye, 2012: Identification and climatology of Southern Hemisphere mobile fronts in a modern reanalysis. *J. Climate*, **25**, 1945–1962, <https://doi.org/10.1175/JCLI-D-11-00100.1>.
- Song, H., Z. Zhang, P. L. Ma, S. J. Ghan, and M. Wang, 2018: An evaluation of marine boundary layer cloud property simulations in the Community Atmosphere Model using satellite observations: Conventional subgrid parameterization versus CLUBB. *J. Climate*, **31**, 2299–2320, <https://doi.org/10.1175/JCLI-D-17-0277.1>.
- Stephens, G. L., and Coauthors, 2002: The *CloudSat* mission and the A-TRAIN: A new dimension to space-based observations of clouds and precipitation. *Bull. Amer. Meteor. Soc.*, **83**, 1771–1790, <https://doi.org/10.1175/BAMS-83-12-1771>.
- Tanelli, S., S. L. Durden, E. Im, K. S. Pak, D. G. Reinke, P. Partain, J. M. Haynes, and R. T. Marchand, 2008: *CloudSat*'s cloud profiling radar after two years in orbit: Performance, calibration, and processing. *IEEE Trans. Geosci. Remote Sens.*, **46**, 3560–3573, <https://doi.org/10.1109/TGRS.2008.2002030>.
- Trenberth, K. E., and J. T. Fasullo, 2010: Simulation of present-day and twenty-first-century energy budgets in the Southern Ocean. *J. Climate*, **23**, 440–454, <https://doi.org/10.1175/2009JCLI3152.1>.
- Wall, C. J., D. L. Hartmann, and P.-L. Ma, 2017: Instantaneous linkages between clouds and large-scale meteorology over the southern ocean in observations and a climate model. *J. Climate*, **30**, 9455–9474, <https://doi.org/10.1175/JCLI-D-17-0156.1>.
- Winker, D. M., M. A. Vaughan, A. H. Omar, Y. Hu, K. A. Powell, Z. Liu, W. H. Hunt, and S. A. Young, 2009: Overview of the *CALIPSO* mission and CALIOP data processing algorithms. *J. Atmos. Oceanic Technol.*, **26**, 2310–2323, <https://doi.org/10.1175/2009JTECHA1281.1>.
- Wood, R., and C. S. Bretherton, 2006: On the relationship between stratiform low cloud cover and lower-tropospheric stability. *J. Climate*, **19**, 6425–6432, <https://doi.org/10.1175/JCLI3988.1>.
- Xiang, B. Q., M. Zhao, Y. Ming, W. D. Yu, and S. M. Kang, 2018: Contrasting impacts of radiative forcing in the Southern Ocean versus southern tropics on ITCZ position and energy transport in one GFDL climate model. *J. Climate*, **31**, 5609–5628, <https://doi.org/10.1175/JCLI-D-17-0566.1>.
- Zhao, M., I. M. Held, S.-J. Lin, and G. A. Vecchi, 2009: Simulations of global hurricane climatology, interannual variability, and response to global warming using a 50-km resolution GCM. *J. Climate*, **22**, 6653–6678, <https://doi.org/10.1175/2009JCLI3049.1>.
- , and Coauthors, 2016: Uncertainty in model climate sensitivity traced to representations of cumulus precipitation microphysics. *J. Climate*, **29**, 543–560, <https://doi.org/10.1175/JCLI-D-15-0191.1>.
- , and Coauthors, 2018a: The GFDL global atmosphere and land model AM4.0/LM4.0: 1. Simulations characteristics with prescribed SSTs. *J. Adv. Model. Earth Syst.*, **10**, 691–734, <https://doi.org/10.1002/2017MS001208>.
- , and Coauthors, 2018b: The GFDL global atmosphere and land model AM4.0/LM4.0: 2. Model description, sensitivity studies, and tuning strategies. *J. Adv. Model. Earth Syst.*, **10**, 735–769, <https://doi.org/10.1002/2017MS001209>.